

Molecule Design for Non-Aqueous Wide-Temperature Electrolytes via the Intelligentized Screening Method

Tian Qin⁺, Haoyi Yang⁺, Lei Wang⁺, Weiran Xue, Nan Yao, Quan Li,* Xiang Chen,*
Xiukang Yang, Xiqian Yu,* Qiang Zhang, and Hong Li

Abstract: Operating a lithium-ion battery (LIB) in a wide temperature range is essential for ensuring a stable electricity supply amidst fluctuating temperatures caused by climate or terrain changes. Electrolyte plays a pivotal role in determining the temperature durability of batteries. However, specialized electrolytes designed for either low or high temperatures typically possess distinct features. Therefore, wide-temperature electrolytes (WTEs) are necessary as they encompass a combination of diverse properties, which complicates the clear instruction of WTE design. Here we represent an artificial intelligence (AI)-assisted workflow of WTE design through stepwise parameterizations and calculations. Linear mono-nitriles are identified as ideal wide-liquidus-range solvents that can “softly” solvate lithium ions by weak interactions. In addition, the explainable modules revealed the halogenoid similarity of cyanide as fluorine on the electrolyte properties (e.g. boiling point and dielectric constant). With the further introduction of an ether bond, 3-methoxypropionitrile (MPN) has been eventually determined as a main electrolyte solvent, enabling the battery operation from –60 to 120 °C. Particularly, a LiCoO₂/Li cell using the proposed WTE can realize stable cycling with capacity retention reaching 72.3 % after 50 cycles under a high temperature of 100 °C.

Introduction

Expanding the application scenarios of LIBs towards wide operating temperatures is one of the important directions of battery development. Unfortunately, The LIB technology based on the liquid electrolytes using LiPF₆ lithium salt and carbonate solvents has a relatively narrow service temperature range (i.e. higher than 0 °C and lower than 60 °C).^[1]

[*] T. Qin,⁺ Dr. H. Yang,⁺ L. Wang,⁺ Dr. W. Xue, Dr. Q. Li, Dr. X. Yu, Prof. H. Li

Beijing Frontier Research Center on Clean Energy
Institute of Physics, Chinese Academy of Sciences
Beijing 100190, China
E-mail: qli@iphy.ac.cn
xyu@iphy.ac.cn

T. Qin,⁺ Dr. W. Xue, Dr. X. Yu, Prof. H. Li
Center of Materials Science and Optoelectronics Engineering
University of Chinese Academy of Sciences
Beijing 100049, China

Dr. N. Yao, Prof. X. Chen, Prof. Q. Zhang
Beijing Key Laboratory of Green Chemical Reaction Engineering
and Technology, Department of Chemical Engineering
Tsinghua University
Beijing 100084, China
E-mail: xiangchen@mail.tsinghua.edu.cn

Prof. X. Yang
Key Laboratory of Environmentally Friendly Chemistry and Applications of Ministry of Education, National Base for International Science & Technology Cooperation, Hunan Province Key Laboratory for Electrochemical Energy Storage and Conversion, School of Chemistry
Xiangtan University
Hunan, Xiangtan 411105, China

[+] These authors contributed equally to this paper

The working temperatures, either too low or too high, have adverse effects on the battery performance and can even lead to safety issues.^[2] This is a striking challenge in most geographic regions on Earth where the environmental temperatures vary considerably due to factors like latitude, altitude, and seasons.^[3] Moreover, space explorations demand battery systems that can withstand extreme temperature fluctuations, reaching up to hundreds of degrees Celsius. To tackle these issues, a temperature control system is commonly employed. However, this does lead to an increase in construction and operation costs.^[4] In fact, the intrinsic wide-temperature operation of batteries primarily relies on the electrolyte. Specifically, the electrolyte which serves as the medium for lithium-ion transportation within the battery and determines the formation of the electrode-electrolyte interphase, has a critical impact on either the low- or high-temperature performance of LIBs. Therefore, improving the wide-temperature performance of LIBs at the electrolyte level is essential and cost-effective for expanding the operation temperature range of LIBs.

When designing low-temperature electrolytes, linear esters or ethers with low viscosity are often preferred because of their superior lithium-ion transport kinetics, and low boiling points. The low ionic conductivity at electrolyte bulk and large desolvation energy penalty are recognized as the main challenges for low-temperature battery operation.^[5] Recently, there has been a significant focus on F-substituted solvents due to their reduced interaction with Li at elevated temperatures. However, these solvents are also known for generating HF at high temperatures, which poses a challenge.^[6] In high-temperature environments, side reactions are exacerbated, leading to the generation of protic species and gases that can be detrimental to the

interface. To address this issue, a high-concentration strategy can be employed in designing high-temperature electrolytes. This approach takes advantage of the beneficial solvation structure to form a strong inorganic-rich interphase that effectively blocks side reactions at elevated temperatures. Nonetheless, it should be noted that the application of this strategy is hindered by high viscosity and interfacial resistance at low temperatures.^[7] It is evident that wide-temperature-range electrolytes (WTEs) present more complex challenges compared to specialized low- or high-temperature electrolytes. This is because WTEs require balancing the unique requirements of both extremes simultaneously.^[8] Furthermore, even simple modifications such as substituting one functional group in solvent molecules can have adverse effects on phase-change temperature and solvation chemistry. Currently, there is a lack of clear instructions for designing WTEs.

Actually, substances that can be potentially used as WTE components vary in huge chemistry space. Researchers have dedicated significant efforts to the design of advanced electrolytes through molecule design for many years, yet there are still numerous unexplored chemical spaces. Besides, the relationship between the structure and performance of an electrolyte molecule in an actual battery system remains ambiguous.^[9] High-throughput methods including calculations and experiments can significantly accelerate the electrolyte design process. The rapidly developed artificial intelligence (AI) methods, such as deep learning, offer significant advantages in processing the resulting large and multi-dimensional data compared with conventional human analysis. The integration of AI can imbue the entire high-throughput process with intelligence for uncovering the underlying principles behind big data. Besides, the key explainability technology turns complex AI models from a “black box” into a “white box”, allowing humans to understand the basis of the model thus providing new perspectives for electrolyte design.

This study has developed an intelligentized screening workflow for the WTE design and identified nitriles as non-fluorinated solvents with a wide liquidus range, high dielectric constant, low viscosity, and low binding energy with lithium ions. These characteristics are essential elements for WTEs. The structure–performance relationship can be established using explainable modules in the trained AI model, which contains over 200 thousand molecules at the level of element and functional group. This reveals the halogenoid similarity of cyanide on the properties of melting point, boiling point, and dielectric constant. Experiments in the next procedure validate the 3-methoxypropionitrile (MPN) as the promising solvent exemplified by high conductivity and anode compatibility. The MPN-based WTE can guarantee the LiCoO₂/Li battery operation over a temperature range of -60 to 120 °C. The concept of “AI for science” as a novel research paradigm has been widely accepted and brought remarkable breakthroughs in the area of biochemistry^[10] and catalysis,^[11] but it is still in its infancy in the fields of LIBs. This work heralds a new paradigm of “AI for battery” for the intelligentized screening accelerating WTE design.

Results and Discussion

An AI-assisted data mining combined with theoretical calculations is proposed to screen the electrolyte solvents of wide operating temperatures. The flow diagram is shown in Figure 1a. Firstly, the molecular properties (i.e. melting points, boiling points, functional groups, etc.) of over 200 thousand molecules with 19 categories were collected and cleaned (the data sources are detailed in Supplementary Note 1). The dataset is utilized to train a model named Molecule VAE, by which the partial missing data in the dataset are complemented automatically via a supervised learning algorithm.^[12] The molecules with a wide liquidus range are of research interest in this dataset of which the amount is decreased to 790. After the elimination of the unsuitable electrolyte molecules (e.g. protic solvents), in the next procedure through theoretical calculations with the consideration of solvation (i.e. solvent, Li salt), the more concerned 16 electrolyte properties, such as binding energy, viscosity, and dielectric constant, are calculated to narrow down the selection range. Finally, the most potential molecules are tested by experiments to decide the target molecules as the wide-temperature electrolyte solvent. At the same time, the explainability technique attached to Molecule VAE is used to analyze the effects of the elements and functional groups on molecular properties, providing new insights for molecular design.

In the training process of the Molecule VAE model, the SMILES (the detail is in Supplementary Note 2) character string of molecules is input into the model through the encoder and decoder modules to reconstruct the input as much as possible (Figure 1b). The high-dimensional and discrete chemical space is compressed into a low-dimensional and continuous coding space through the encoder. The learning latent space blends molecular structure information, which can be directly used as characteristics to predict without the need for complex feature engineering.^[13] Furthermore, the processes of learning latent space and prediction are separated. The data needed for training latent space is massive molecular SMILES, but the data of corresponding properties needed for the predictor is not necessarily large. Therefore, the different data is used hierarchically by the transfer learning method, i.e., big data for training and small data for fine-tuning. 88.5 % and 84.6 % of categorical accuracy for SMILES prediction, and the values of root mean square error between the prediction and truth are 61.08 and 84.39 K are maintained in the boiling point and melting point test datasets, respectively (Figure 1c, S1, and Supplementary Note 2), which manifests the high predictive accuracy of the model.

790 molecules with molar weight less than 150 g mol⁻¹, boiling point higher than 80 °C, and melting point lower than -40 °C are chosen as the wide liquidus range molecules from 200 thousand ones (Figure 1d). Based on the functional group characteristics, the molecules unsuitable as electrolyte solvents are excluded, such as protic solvents or polymer monomers (the classification details are shown in Table S1 and Supplementary Note 3). 24 potential wide-temperature molecules sieved out from the database are further eval-

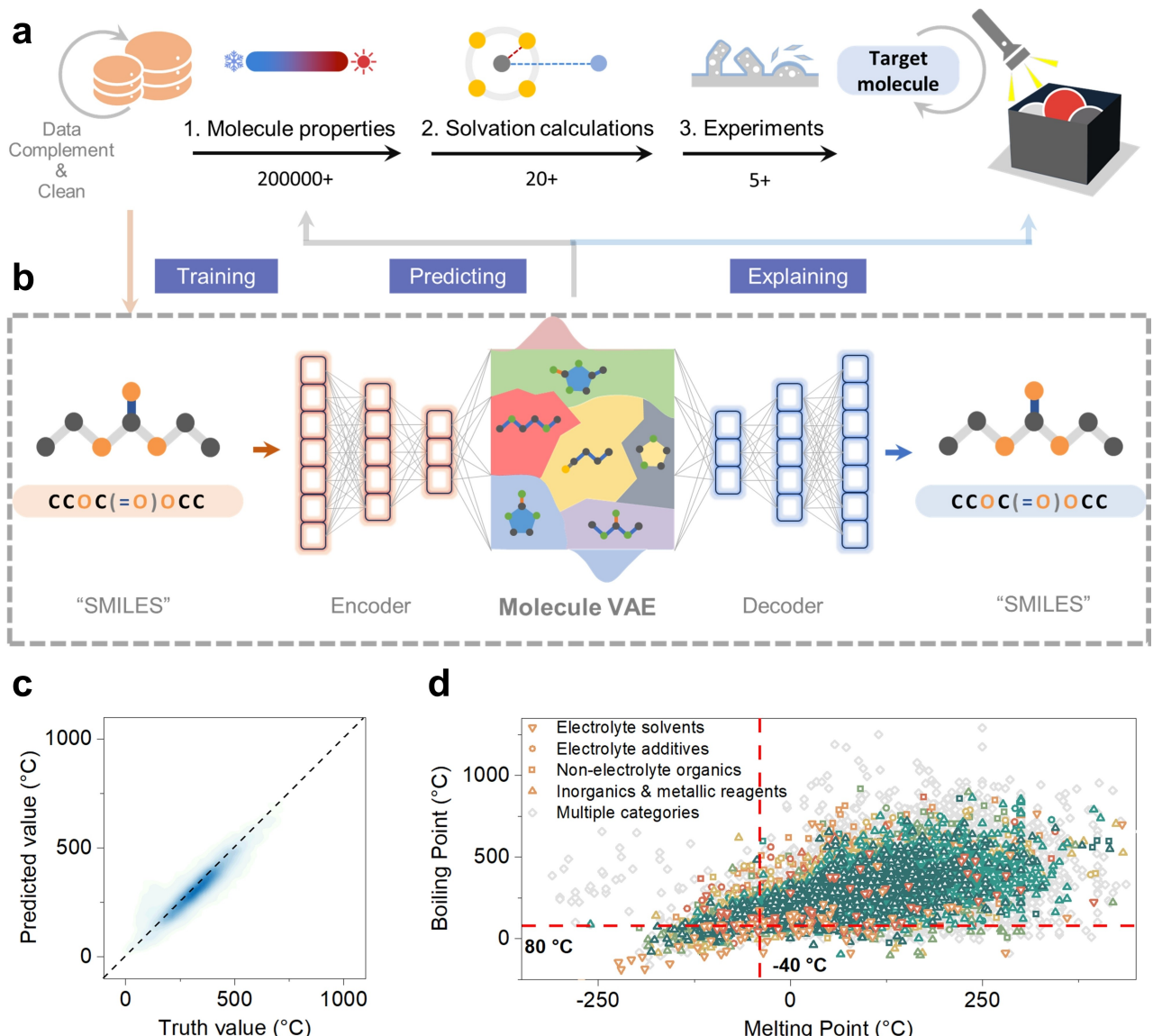


Figure 1. The construction of molecular database and screening workflow. (a) The workflow of AI-assisted screening of the wide-temperature electrolytes. (b) The model architecture of Molecule VAE. (c) Truth versus prediction plots of boiling points for Molecule VAE. (d) The distribution of melting point and boiling point data. The molecules are classified into four categories based on the functional group characteristics as shown in Table S1.

uated by both functional theory (DFT) calculations and molecular dynamics (MD) simulations. 16 solvation properties that directly affect the battery performance are obtained, including binding energy, viscosity, dielectric constant, conductivity, HOMO and LUMO energy level, and transference number (Figure S2–4).^[14] High dielectric constant reflects the excellent ability of a solvent to solvate lithium-ions. Low binding energy can reduce the desolvation energy of lithium ions and increase the number of anions in the solvent structure that contributes to anion-derived inorganic SEI.^[15] As plotted in Figure 2a, several linear nitriles are predicted to simultaneously possess low viscosity, high dielectric constant, and low binding energy, which are termed the “soft solvating” solvents. Such “soft” eloquently shows the large polarizability and weak electron-donating

property, which is similar to the concept of a “soft” Lewis base.^[16] Furthermore, the nitriles known as common high voltage solvents or additives have the lowest HOMO levels in terms of pure solvents (Figure S2b), while after forming a cluster with Li salt the situations are changed (Figure S2d), which highlights the consideration of cluster formation in actual electrolytes.^[17] The nitriles, especially with short carbon chains, have low viscosity and high conductivity. As for the transference number, the values fluctuate around 0.5 as a typical phenomenon in liquid electrolytes (Figure S2–4).

Even with powerful fitting and predictive ability, deep learning models are too complex to be understood, which is a common problem for big models. To clarify the role of element and functional groups, the Local Interpretable Model-Agnostic Explanations (LIME) method is used on

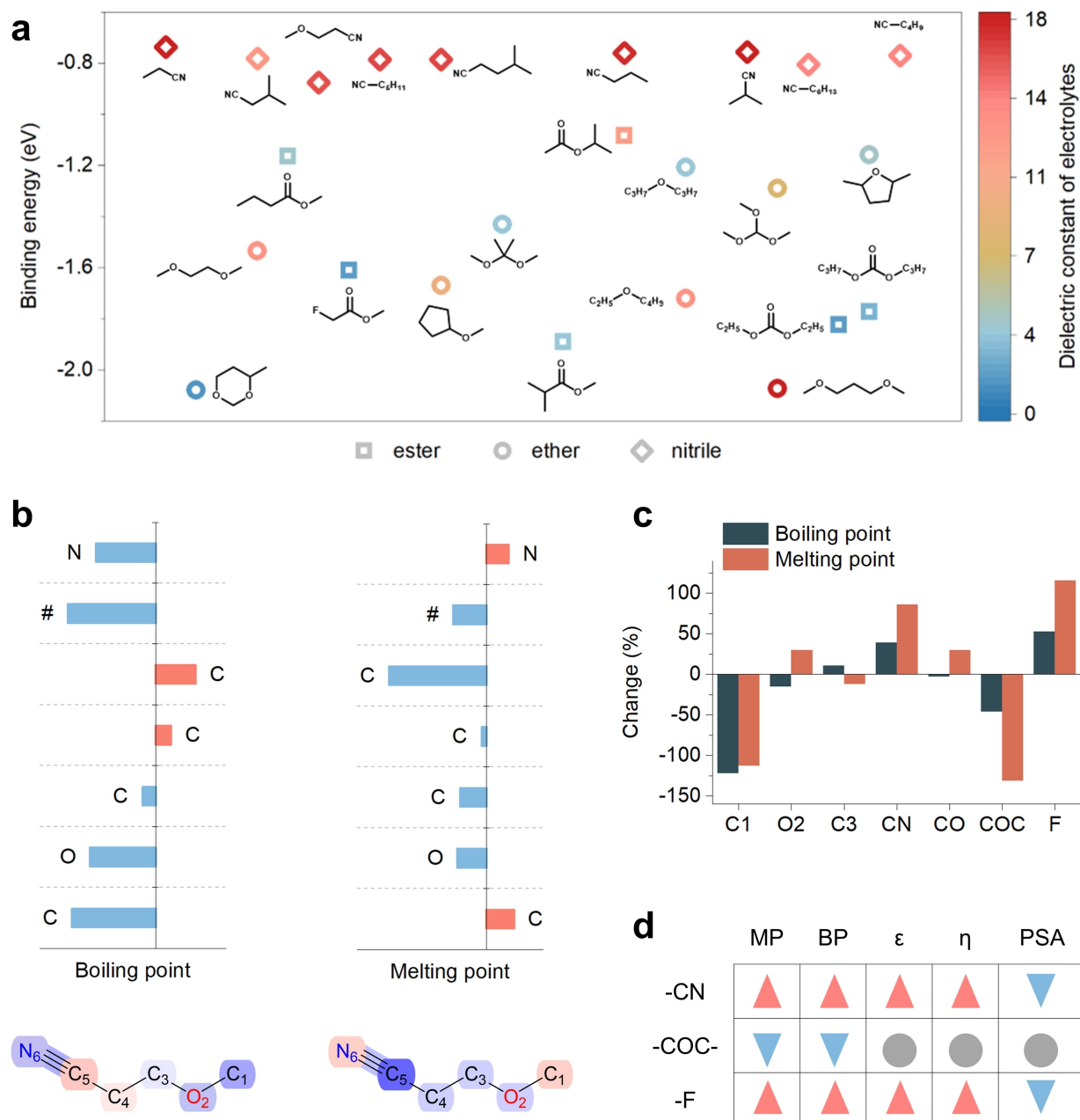


Figure 2. The theory calculations of potential molecules and explainable analysis for AI model. (a) The distribution of binding energy and dielectric constant of the sieved molecules. The Y-axis is binding energy. The color of the marks represents dielectric constants. (b) The effect of each atom on the boiling point and melting point based on the explainable analysis. The abscissa represents the relative importance without a physical unit. '#' belonging to SMILES characteristics represents the triple bonds. In the schematic molecule, the bluer color represents a more negative effect and the redder color represents a more positive effect. (c) The change of boiling and melting point after removing different atoms and functional groups. (d) The influence of cyanide group ($-CN$), ether bonds ($-COC-$), and fluorination ($-F$) on the MP (melting point), BP (boiling point), ϵ (dielectric constant), and η (viscosity) of molecules. The red upward triangles, the blue downward triangles, and the grey circles represent a positive effect, a negative effect, and an insignificant effect, respectively.

Molecule VAE to explain the prediction behavior. The LIME method explains complex models by the simple explainable models (e.g., ridge regression models) as surrogate models, which are fitted with the data randomly sampled around a selected sample to explain local behaviors for prediction. The model's understanding of the effect of each element on the melting boiling point is examined

through the LIME method (Figure S5a, the detail is in Supplementary Note 4). We also check the impact of the volume of the input dataset. It is found that after increasing the volume of the training database, the predicted results show similar effects of all elements statistically compared to limited data for training with bias (Figure S5b).

To understand the structure–performance relationship of the molecules among nitriles, we chose MPN as an example, which contains several elements for explainable analysis and the optimal performance to be discussed later. The contribution of every positioned atom in MPN to the boiling point and melting point can be measured quantitatively by explainable methods (Figure 2b). Meanwhile, the importance of the functional groups for the boiling point and melting point is obtained via ablation experiments, i.e. the change of corresponding properties after removing the functional groups (Figure 2c). It can be seen that the polar cyanide group ($-\text{CN}$) of MPN is beneficial for lifting boiling point and melting point, but ether bond ($-\text{COC}-$) does the opposite which counters the raised melting point and broaden the liquidus range. The similar trend is seen for other nitrile molecules (Figure S6). Fluorination has recently been a popular method of solvent molecular design.^[18] When replacing cyanide groups with one fluorine, the molecule has similar trends of boiling point and melting point to the cyanide group. Utilizing similar methods, the influence of atoms and function groups on polar surface area (PSA), viscosity, and dielectric constant is measured quantitatively as shown in Figure S7. The influence of the cyanide group, ether bonds, and fluorination on each property is summarized in Figure 2d. The polar surface area is the surface belonging to polar atoms, which is related to the polarity of molecules, and is widely used as a quantitative descriptor to compare the transport properties of drugs in biology.^[19] The polarity is of importance to affect the properties of molecule, including the basically physical properties and the solvent properties. Previous researches have proven the weak polarity is beneficial to weakening the binding energy between the solvent and lithium ions.^[1] Therefore, PSA is also collected to represent the similarity of cyanide group and fluorination, i.e. both to decrease the PSA of molecules. The molecules substituted by cyanide group or fluorine atoms both can “softly” solvate lithium ions by weak interactions as the binding energy decrease (Figure S8). The cyanide group indicates a similar function compared to fluorination, which proves the halogenoid property of the cyanide group.

Explainable technique comprehends the complex AI models and guides us to molecular design according to the rules obtained from training on the massive data. As shown in Figure 3a, simple alkane molecules have extremely low melting points, boiling points, and dielectric constants, which are unable to solvate lithium ions and therefore not suitable as electrolyte solvents. When introducing one electron-donating oxygen atom into the alkane backbone, the ether gains a relatively wider liquidus range and higher dielectric constant. Ether can be used as a solvent with satisfactory solvation ability, but may not tolerate wide temperatures, such as 1,2-dimethoxyethane ($-58\text{--}82^\circ\text{C}$) with high saturated vapor pressure. Inspiringly, the introduction of the cyanide group can significantly improve the liquidus range and dielectric constant.

Based on the calculation results, a series of linear mono-substituted nitriles are sieved out. We further verified the differences in nitriles through experiments. Butyronitrile^[20]

and isobutyronitrile^[21] have been reported as the solvent of ultralow temperature electrolytes ($< -70^\circ\text{C}$). Propionitrile is highly toxic and is strictly controlled. In that sense, these three nitriles are not for consideration here. The residual 6 nitriles have very similar physiochemical properties in the theory calculations. To screen the available solvents, facile experiments were conducted. All 6 pure nitrile solvents reacted violently with lithium metal, but this reaction is suppressed when lithium salts are added (Figure S9). Among the nitrile solvents with 1 M LiTFSI, MPN electrolyte shows the highest conductivity from 25 to -40°C (Figure 3b). This could be attributed to the ether group that aids the Li solvation even when the binding energy is low. In the infrared spectrum (Figure 3c), the peak of the cyanide group is at 2250 cm^{-1} and the newly emerged peak after coordination with lithium ions is positioned at about 2275 cm^{-1} . In the MPN solution, the highest peak ratio of free solvent/coordinated solvent proves that MPN has a relatively weak Li interaction. It is surprising that except for MPN, which has an additional ether bond, the available capacities of other nitrile electrolytes are very low in Li/Cu and LCO half cells (Figure S10–11).

Nitrile-based molecules are known for their high voltage stability and good affinity with the surface metal center of cathode materials, which prevents side reactions at the cathode surface.^[22] Furthermore, linear nitriles have considerably high ionic conductivity with a unique mechanism.^[23] Despite the potential of wide-temperature application, little is known about the properties of MPN solvent at a molecule level.

MPN is mixed with PC as the SEI-forming co-solvent and LiTFSI is chosen as the main salt due to its high dissociation constant, thermostability, and superior chemical stability. The ratio of solvents is optimized to balance the low- and high-temperature performances (Figure S12). The conductivities and viscosities of conventional carbonate EC/DEC electrolyte (COE) and MPN/PC electrolyte (WTE) from -50°C to room temperature are plotted in Figure 3d. WTE electrolyte has an even higher ionic conductivity (7.93 mS/cm) than EC/DEC (7.66 mS/cm) at room temperature. At a low temperature of -50°C , WTE has much lower viscosity (115 mPa·s) than COE (472 mPa·s) and higher conductivity (0.373 mS/cm) than COE (0.142 mS/cm), which indicates the low inter-molecule and inter-ionic interaction of MPN electrolyte. The differential scanning calorimetry (DSC) tests reveal that WTE has lower heat release (0.2 W/g) than COE (1.7 W/g), which indicates better high-temperature thermostability (Figure 3e).

Furthermore, by recording the motion trajectories of various molecules and ions during the MD simulation, the radial distribution functions (RDF) of the solvation structures in the two electrolytes and their corresponding coordination numbers are obtained (Figure S13). The considerable MPN ratio in the solvation structure results from the moderate donor number (15.4)^[24] and relatively high dielectric constant. The relatively weak ion–solvent interaction of MPN invests WTE with low desolvation energy, which is critical for improving low-temperature interfacial reaction kinetics.

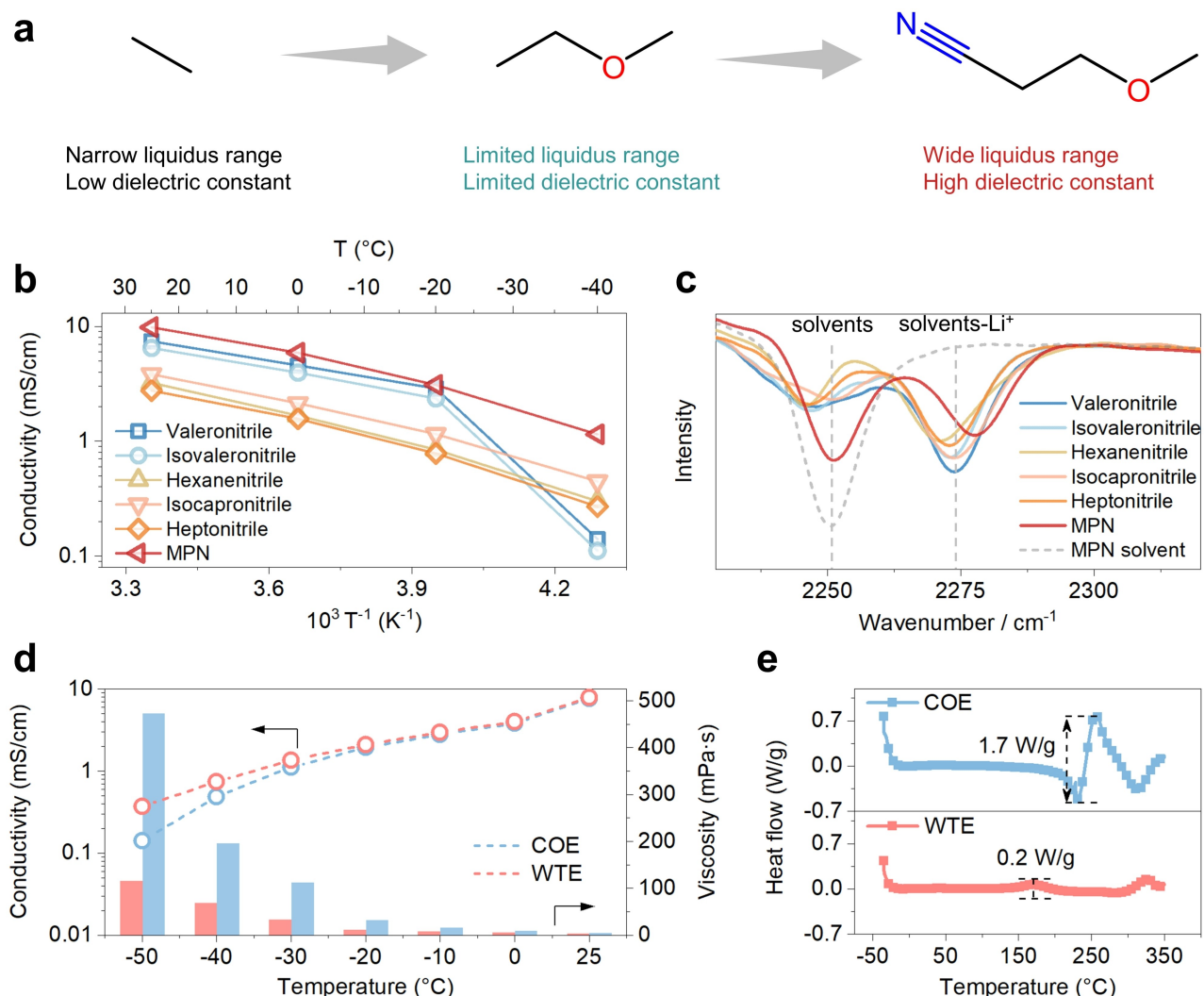


Figure 3. The measured electrolyte properties of nitrile solvents. (a) The molecule design flow. (b) The conductivities of nitrile solutions from -40 to 25 °C. (c) The Infrared spectra of nitrile solutions. (d) The conductivities and viscosities of the COE and WTE across wide temperatures. (e) DSC curves of COE and WTE from -40 to 350 °C.

The linear sweep voltammetry (LSV) results confirm that the WTE has an electrochemical window over 4.9 V (Figure S14). It proves this electrolyte has resistance to high-voltage oxidation, which agrees with previous calculations. The WTE electrolyte exhibited no significant corrosion current at an elevated temperature of 80 °C (Figure S15), demonstrating a well-passivated interphase of the Al current collector (Figure S16).

We further assess the room- and low-temperature electrochemical performances of LiCoO₂/Li cells using WTE in comparison with COE (Figure 4a). At room temperature, COE and WTE achieved similar specific discharge capacities (139 mAh g⁻¹) (Figure S17). Superior cycling performance and rate capability are realized in WTE compared to the COE electrolyte (Figure S18). Furthermore, WTE supports a high cut-off voltage of 4.5 V cycling (Figure S19). When the temperature is decreased, the COE electrolyte exhibits a rapid capacity decay. At -30 °C, the capacity is only 54.7 % of that at room temperature, and when the temperature

further drops below -40 °C, there is nearly no capacity delivered. In contrast, the WTE electrolyte displays impressive low-temperature performance. At -30 °C, it has a discharge capacity of 115 mAh g⁻¹, which is 82.4 % of the room temperature capacity. Even as the temperature is lowered to -50 and -60 °C, it still provides approximately 65.4 % and 39.1 % of the room temperature capacity, respectively. In addition, the cells with WTE can be cycled well at -20 °C (Figure S20).

For the high-temperature performances, as shown in Figure 4b, there are pronounced differences in the electrochemical performance between the two electrolytes at high temperatures. At 60 °C, the LiCoO₂/Li battery using the COE experiences a rapid capacity decline after 60 cycles, with a capacity retention of only 57.9 % after 150 cycles. In contrast, the battery using the WTE at 60 °C maintains good cycle stability, with a capacity retention of 93.4 % after 150 cycles, significantly higher than the COE. Furthermore, at 80 °C, the LiCoO₂/Li battery with the COE suffers rapid

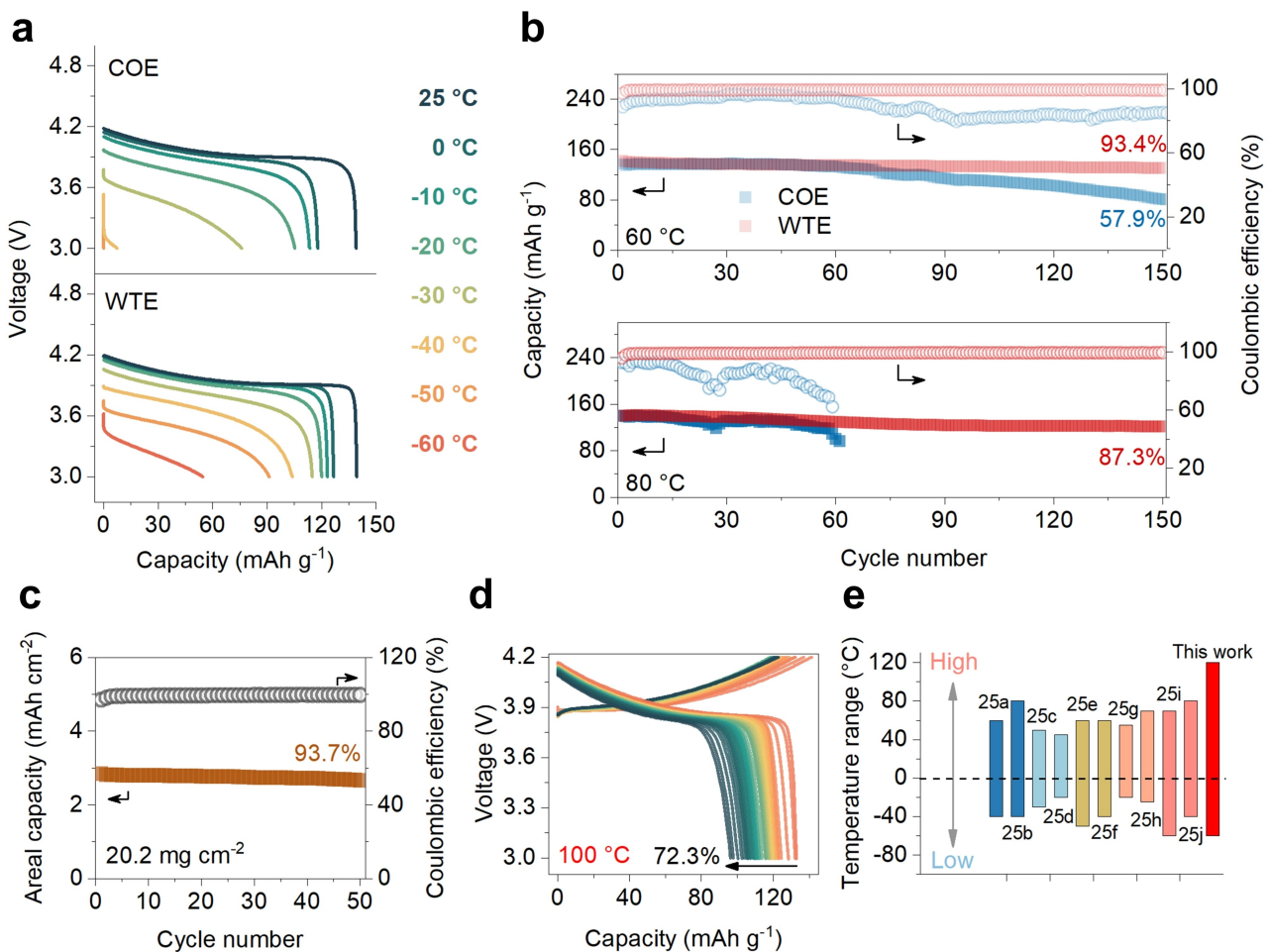


Figure 4. The electrochemical performance of the WTE electrolyte at a wide temperature range. (a) The discharge curves of LiCoO₂/Li cells using COE and WTE as electrolytes at low temperatures at a current density of 0.1 C (1 C = 140 mAh g⁻¹). (b) The discharge capacity and the Coulombic efficiency of LiCoO₂/Li cells with COE and WTE cycling at elevated temperatures of 60 and 80 °C at a current density of 1 C. (c) The cycling performance of cells with a high mass loading of 20.2 mg cm⁻² using WTE at room temperature at a current density of 0.1 C. (d) The voltage curves of cells after 50 cycles under 100 °C using WTE at a current density of 2.5 C. (e) Comparison of the operating temperature ranges of the LIBs reported in recent literature. The number in the figure corresponds to the reference sequence. From left to right, the different color columns represent the different electrolyte categories: high-concentration electrolytes (and local high-concentration electrolytes), S-containing additives, nitrile-containing additives, borate and phosphate-containing additives, and others.

capacity loss, with a capacity retention of only 56.7 % after 92 cycles. In contrast, the battery using the WTE demonstrates an impressively stable cycling performance, with a capacity retention of 87.3 % after 150 cycles. Notably, the Coulombic efficiency (CE) of the WTE (average CE of 99.2 %) is also significantly higher than that of the COE (average CE of 69.4 %), indicating the reduced side reactions with WTE at high temperatures. The capacity retention of cells with 20.2 mg cm⁻² mass loading using WTE reaches 93.7 % after 50 cycles (Figure 4c). Under extreme operating conditions, including a high temperature of 100 °C, WTE can also realize the cell's cycling, and the capacity retention reaches 72.3 % after 50 cycles (Figure 4d). Besides, at higher temperature (120 °C, Figure S21), and higher voltage (4.4 V with 60 or 80 °C, Figure S22), WTE can also retain the outstanding cycle stability.

The operating temperature range of this work is compared with recently reported literature (Figure 4e) and

the capacity retention at low and high temperatures is compared in Table S2 and Figure S23.^[25] We have realized the operation from -60 to 100 °C, the stable cycling from -20 to 80 °C and satisfactory capacity retention at either low or high temperatures. The operation temperature from -60 to 100 °C is wider to most works with liquid electrolyte no matter what material systems.

To clarify the origin of superior low- and high-temperature performances for WTE, electrochemical impedance spectroscopy (EIS) was conducted to quantify the reaction impedances at different temperatures (Figure S24a and Figure S25). Compared to the COE, the cell using the WTE always exhibits lower impedances. Both of the activation energy for the ion transport across SEI and the desolvation energy in the WTE are lower than COE (Figure S24b). This points to the lower kinetic barrier in the WTE than in the COE, underlying a substantial improvement in low-temperature performances. At a high temperature of 80 °C, the cells

using COE exhibit a notable increase in impedance compared to WTE (Figure S26), which can be attributed to the severe side reactions and accumulation of decomposition products at the surface of the electrodes.^[26] The concentration of Co²⁺ in cycled cells with COE is 7.2 times higher than that with WTE further, which supports this finding (Figure S27). This suggests that a rather small amount of Co is leached from the cathode structure while the migration of Co to the anode and the catalysis of solvent decomposition are the main reasons for the reduced high-temperature

stability.^[27] Therefore, the interface stability between the cathode and the electrolyte should be emphasized.

For the lithium metal anode, the deposition morphology of lithium metal has a significant impact on long-cycle interface stability. The lithium deposits at high temperature and room temperature are shown in Figure 5a–c and Figure S28. At both high temperature and room temperature in the COE, lithium metal anode exhibits a loose and porous morphology with a high specific surface area. In contrast, a different morphology is observed for the WTE. Lithium metal mostly exists in the form of larger micrometer-sized

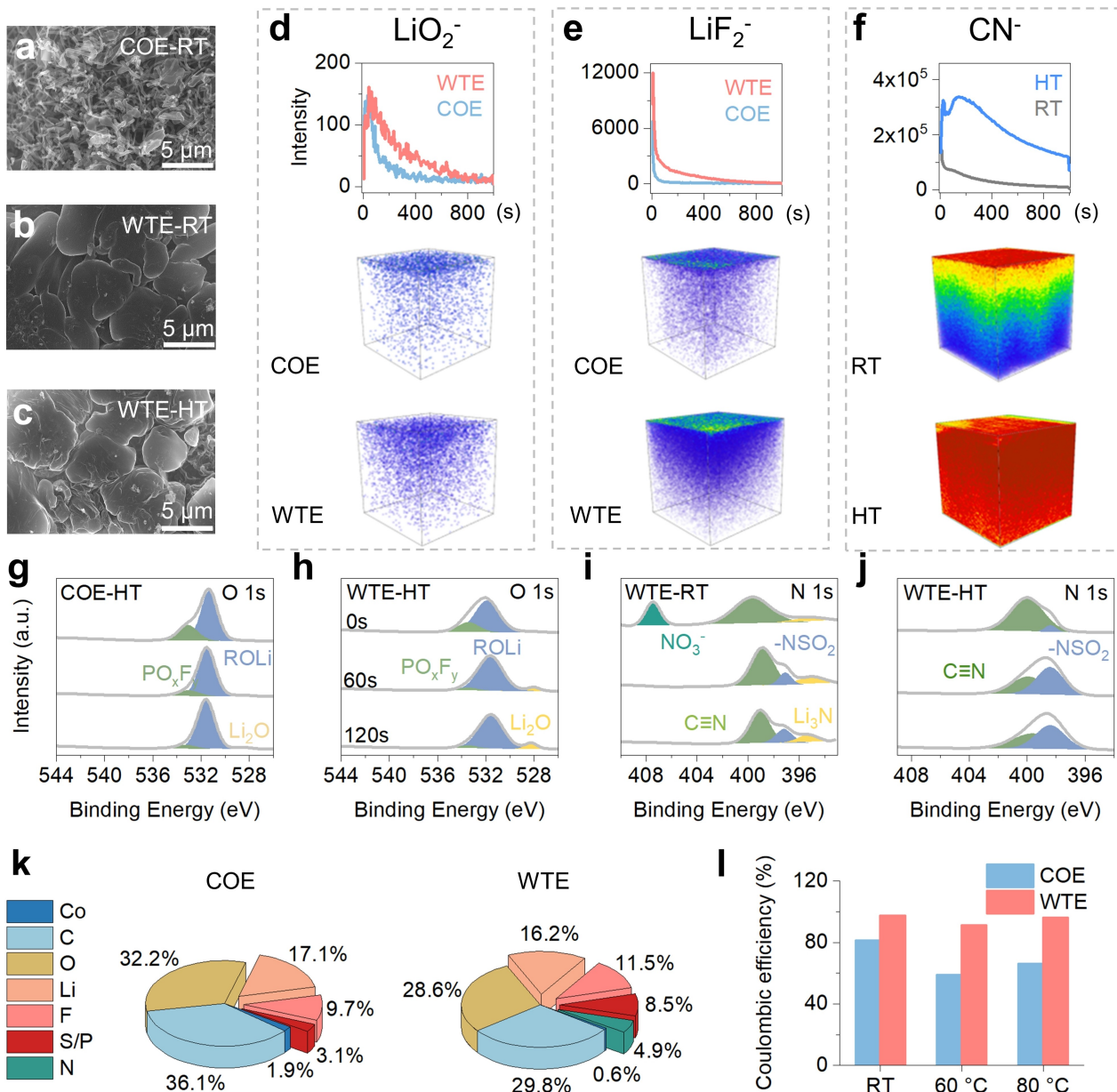


Figure 5. The interphase components formed at different temperatures. The surface morphology of lithium metal anodes after 50 cycles at 25 °C (Room temperature, RT) with (a) COE and (b) WTE, and (c) 60 °C (High temperature, HT) with WTE. The distribution of (d) LiO₂⁻, and (e) LiF₂⁻ on the lithium surface with WTE and COE at RT. (f) The distribution of CN⁻ on the lithium surface with WTE at RT and HT. XPS depth profiling results of O 1s spectra at HT with (g) COE and (h) WTE. XPS depth profiling results of N 1s spectra with WTE at (i) RT and (j) HT. (k) The chemical composition ratio of the surface of lithium metal anodes using COE and WTE at HT. (l) Coulombic efficiency measurements of Li/Cu cells with WTE and COE using the Aurbach method at RT, 60, and 80 °C.

blocky particles (5–10 μm, Figure 5b and 5c), resulting in a significantly reduced specific surface area. Furthermore, COE forms a thicker lithium deposition layer (11.5 μm, Figure S28b) containing insoluble byproducts and dead lithium after 50 cycles which increases the battery impedance. However, the WTE maintains a thinner deposited lithium layer (5.2 μm) after 50 cycles (Figure S28a).

The chemical compositions of the SEI formed on the lithium metal anode at room and high temperature are analyzed using XPS depth profiling and TOF-SIMS (time-of-flight secondary ion mass spectrometry) (Figure 5d–j). The results demonstrate a higher concentration of Li₂O and LiF distributed in SEI of WTE than COE (Figure 5d–e). It has been reported the Li₂O-dominated SEI (Figure 5g–h) has better properties to reduce lithium ion diffusion energy barriers and high-temperature stability.^[28] On the one hand, the Li₃N and Li₂O ingredients enable the interphase formed in the WTE electrolyte to maintain a relatively high ion transportation ability even at low temperatures, thereby improving the low-temperature performance of the battery. On the other hand, the LiF and Li₂O ingredients ensure the thermal/chemical stability of anode and cathode interphases, protecting them from side reactions (e.g. HF attack) at high temperatures. (Figure S29–37). In contrast, the SEI formed in the COE electrolyte maintains a high level of C and O elements throughout the entire depth profile, especially at high temperatures (Figure 5k and S29–30), which is consistent with the distribution of organic species (e.g. C₂HO⁻) in Figure S33–34.

It is worth noting that there are evident differences in the type and proportion of N 1s signals between the interphases (both SEI and CEI) at room temperature and high temperature, which suggests the different decomposition mechanisms of nitrogen-containing components at varied temperatures.^[29] The cyanide group in MPN processes relatively reductive activity, which may generate oligomer and polymer to modify the SEI or CEI on the electrode surface (proposed reaction paths in Figure S38). Anyhow, the adsorption of CN⁻ from MPN is effective in protecting the interphase from fierce side reactions, especially at high temperatures (Figure 5f and S39). There are more cyanides and –NSO₂ signals at higher temperatures (Figure 5i–j and S39). The different SEI (or CEI) formation paths at changed temperatures will be of great importance to the rational design of wide-temperature electrolytes that are expected to form stable interphase over a wide temperature range. As for the CEI on LiCoO₂, (Figure S36 and S40) the high nitrogen content (>4.5 %) dominated by C≡N on the cathode surface for WTE electrolyte evidences the critical role of the MPN solvent. Cyanide groups (C≡N) from the solvent MPN, with a strong coordination ability, are prone to adsorb on metal sites on the cathode surface and possibly inhibit the reaction of other components of the electrolyte by the cathode (e.g. dehydrogenation of solvent). Therefore, the thin inorganic-rich interphase formed on both the cathode and anode ensures excellent performances across a wide temperature.

To describe the compatibility between the electrolyte and lithium metal anode, the Coulombic efficiency is

precisely determined in Li/Cu cells using the method proposed by Aurbach.^[30] The Coulombic efficiency of the WTE electrolyte is 97.2 % at room temperature and 91.1 % at 60°C, significantly higher than the 81.3 % and 58.8 % achieved with the COE electrolyte (Figure 5l and S41). This confirms that the interphase formed on the lithium metal anode exhibits good passivation ability.

Conclusion

In summary, we have established a molecule database consisting of physicochemical properties through AI-assisted processing by which the model yields multi-dimensional prediction. To select a solvent molecule suitable for WTEs, the liquidus range of the molecules is firstly focused on with model analysis. Guided by the explainable model, the contributions of constitution functional groups are unfolded, which comprehend the understanding of the structure–performance relationship to reveal the halogenoid property of cyanide. After theoretical calculations of lithium-ion solvation chemistry, the linear nitriles have been screened out as electronically soft solvents with high dielectric constants yet a weak binding ability to lithium ions. Further introduction of ether group leads to stable interphase formation and optimal solvating ability. The electrolyte with MPN as the main solvent enables a wide operating temperature of LIBs from –60 to 120°C. This LiCoO₂/Li cell using WTE has capacity retention of 82.4 % of the room-temperature capacity at a low temperature of –30°C, and even 65.4 % at –50°C. Moreover, it exhibits stable performance even at a high temperature of 80°C, with a capacity retention of 87.3 % after 150 cycles, and even 72.3 % at 100°C after 50 cycles. The low binding energy of MPN with lithium ions enables the fast desolvation process at low temperatures and the formation of inorganic interphase ingredients to shelter side reactions at high temperatures. Hopefully, the AI-assisted methodology can accelerate the electrolyte design with multi-dimensional instructions and disentangle the complicated structure–performance relationship, for instance, understanding the inter- and intra-molecule interactions in practical electrolytes.

Supporting Information

The authors have cited additional references within the Supporting Information.^[31–42]

Acknowledgements

The work was supported by funding from the National Natural Science Foundation of China (grant no. 52325207, 22239003, T2322015), Beijing Municipal Science & Technology Commission (Z221100006722015), National Key Research and Development Program (2021YFB2500300), and CAS Project for Young Scientists in Basic Research (Grant No. YSBR-058).

Conflict of Interest

The authors declare no conflict of interest.

Data Availability Statement

The data that support the findings of this study are available from the corresponding author upon reasonable request.

Keywords: AI-assisted screening method · wide-temperature electrolyte · lithium-ion batteries · molecular design · big data

- [1] Y. Feng, L. Zhou, H. Ma, Z. Wu, Q. Zhao, H. Li, K. Zhang, J. Chen, *Energy Environ. Sci.* **2022**, *15*, 1711–1759.
- [2] J. M. Tarascon, M. Armand, *Nature* **2001**, *414*, 359–367.
- [3] S. R. Loarie, P. B. Duffy, H. Hamilton, G. P. Asner, C. B. Field, D. D. Ackerly, *Nature* **2009**, *462*, 1052–1055.
- [4] M. Hao, J. Li, S. Park, S. Moura, C. Dames, *Nat. Energy* **2018**, *3*, 899–906.
- [5] X. Dong, Y.-G. Wang, Y. Xia, *Acc. Chem. Res.* **2021**, *54*, 3883–3894.
- [6] C.-B. Jin, N. Yao, Y. Xiao, J. Xie, Z. Li, X. Chen, B.-Q. Li, X.-Q. Zhang, J.-Q. Huang, Q. Zhang, *Adv. Mater.* **2023**, *35*, 2208340.
- [7] M. Zhang, J. Zhang, J. Yang, J. Yao, Z. Chen, C. Lu, X. Du, Z. Zhang, H. Zhang, G. Cui, *Chem. Commun.* **2019**, *55*, 9785–9788.
- [8] A. Pan, Z. Wang, F. Zhang, L. Wang, J. Xu, J. Zheng, J. Hu, C. Zhao, X. Wu, *Nano Res.* **2022**, *16*, 8260–8268.
- [9] N. Yao, X. Chen, Z.-H. Fu, Q. Zhang, *Chem. Rev.* **2022**, *122*, 10970–11021.
- [10] H. A. Elmarakeby, J. Hwang, R. Arafah, J. Crowdus, S. Gang, D. Liu, S. H. AlDubayan, K. Salari, S. Kregel, C. Richter, T. E. Arnoff, J. Park, W. C. Hahn, E. M. Van Allen, *Nature* **2021**, *598*, 348–352.
- [11] J. P. Reid, M. S. Sigman, *Nature* **2019**, *571*, 343–348.
- [12] R. Gómez-Bombarelli, J. N. Wei, D. Duvenaud, J. M. Hernández-Lobato, B. Sánchez-Lengeling, D. Sheberla, J. Aguilera-Iparraguirre, T. D. Hirzel, R. P. Adams, A. Aspuru-Guzik, *ACS Cent. Sci.* **2018**, *4*, 268–276.
- [13] L.-C. Xu, J. Frey, X. Hou, S.-Q. Zhang, Y.-Y. Li, J. C. A. Oliveira, S.-W. Li, L. Ackermann, X. Hong, *Nat. Synth.* **2023**, *2*, 321–330.
- [14] Y.-C. Gao, N. Yao, X. Chen, L. Yu, R. Zhang, Q. Zhang, *J. Am. Chem. Soc.* **2023**, *145*, 23764–23770.
- [15] J. Xu, J. Zhang, T. P. Pollard, Q. Li, S. Tan, S. Hou, H. Wan, F. Chen, H. He, E. Hu, K. Xu, X.-Q. Yang, O. Borodin, C. Wang, *Nature* **2023**, *614*, 694–700.
- [16] G. Gritzner, *J. Mol. Liq.* **1997**, *73*–*74*, 487–500.
- [17] E. R. Fadel, F. Faglioni, G. Samsonidze, N. Molinari, B. V. Merinov, W. A. Goddard III, J. C. Grossman, J. P. Mailoa, B. Kozinsky, *Nat. Commun.* **2019**, *10*, 3360.
- [18] Y. Wang, Z. Li, Y. Hou, Z. Hao, Q. Zhang, Y. Ni, Y. Lu, Z. Yan, K. Zhang, Q. Zhao, F. Li, J. Chen, *Chem. Soc. Rev.* **2023**, *52*, 2713–2763.
- [19] P. Ertl, B. Rohde, P. Selzer, *J. Med. Chem.* **2000**, *43*, 3714–3717.
- [20] J. Gai, J. Yang, W. Yang, Q. Li, X. Wu, H. Li, *Chin. Phys. Lett.* **2023**, *40*, 086101.
- [21] L. Luo, K. Chen, H. Chen, H. Li, R. Cao, X. Feng, W. Chen, Y. Fang, Y. Cao, *Adv. Mater.* **2023**, *36*, 2308881.
- [22] X. Yang, M. Lin, G. Zheng, J. Wu, X. Wang, F. Ren, W. Zhang, Y. Liao, W. Zhao, Z. Zhang, N. Xu, W. Yang, Y. Yang, *Adv. Funct. Mater.* **2020**, *30*, 2004664.
- [23] D. Lu, R. Li, M. M. Rahman, P. Yu, L. Lv, S. Yang, Y. Huang, C. Sun, S. Zhang, H. Zhang, J. Zhang, X. Xiao, T. Deng, L. Fan, L. Chen, J. Wang, E. Hu, C. Wang, X. Fan, *Nature* **2024**, *627*, 101–107.
- [24] S. Venkatesan, I. P. Liu, C.-W. Li, C.-M. Tseng-Shan, Y.-L. Lee, *ACS Sustainable Chem. Eng.* **2019**, *7*, 7403–7411.
- [25] a) X. Zhang, L. Zou, Y. Xu, X. Cao, M. H. Engelhard, B. E. Matthews, L. Zhong, H. Wu, H. Jia, X. Ren, P. Gao, Z. Chen, Y. Qin, C. Kompella, B. W. Arey, J. Li, D. Wang, C. Wang, J.-G. Zhang, W. Xu, *Adv. Energy Mater.* **2020**, *10*, 2000368; b) J. Li, H. Hua, X. Deng, P. Lai, Y. Kang, S. Kuang, F. Wang, X. Zeng, Y. Zhang, J. Zhao, *Chem. Eng. J.* **2023**, *452*, 139398; c) X. Lan, S. Yang, T. Meng, C. Zhang, X. Hu, *Adv. Energy Mater.* **2023**, *13*, 2203449; d) J. Lu, X. Xu, W. Fan, Y. Xin, W. Wang, C. Fan, P. Cheng, J. Zhao, J. Liu, Y. Huo, *ACS Appl. Energ. Mater.* **2022**, *5*, 6324–6334; e) Y. Zou, Z. Ma, G. Liu, Q. Li, D. Yin, X. Shi, Z. Cao, Z. Tian, H. Kim, Y. Guo, C. Sun, L. Cavallo, L. Wang, H. N. Alshareef, Y.-K. Sun, J. Ming, *Angew. Chem. Int. Ed.* **2023**, *62*, e202216189; f) Y. Zou, G. Liu, Y. Wang, Q. Li, Z. Ma, D. Yin, Y. Liang, Z. Cao, L. Cavallo, H. Kim, L. Wang, H. N. Alshareef, Y.-K. Sun, J. Ming, *Adv. Energy Mater.* **2023**, *13*, 2300443; g) Z. Lu, D. Liu, K. Dai, K. Liu, C. Jing, W. He, W. Wang, C. Zhang, W. Wei, *Energy Storage Mater.* **2023**, *57*, 316–325; h) Y. Wang, H. Zheng, L. Hong, F. Jiang, Y. Liu, X. Feng, R. Zhou, Y. Sun, H. Xiang, *Chem. Eng. J.* **2022**, *445*, 136802; i) Z. Wang, H. Zhang, J. Xu, A. Pan, F. Zhang, L. Wang, R. Han, J. Hu, M. Liu, X. Wu, *Adv. Funct. Mater.* **2022**, *32*, 2112598; j) A. Wang, Y. Song, Z. Zhao, X. Li, Z. Hu, J. Luo, *Adv. Funct. Mater.* **2023**, *33*, 2302503.
- [26] C. Zhan, T. Wu, J. Lu, K. Amine, *Energy Environ. Sci.* **2018**, *11*, 243–257.
- [27] T. Joshi, K. Eom, G. Yushin, T. F. Fuller, *J. Electrochem. Soc.* **2014**, *161*, A1915–A1921.
- [28] a) H. Zeng, K. Yu, J. Li, M. Yuan, J. Wang, Q. Wang, A. Lai, Y. Jiang, X. Yan, G. Zhang, H. Xu, J. Wang, W. Huang, C. Wang, Y. Deng, S.-S. Chi, *ACS Nano* **2024**, *18*, 1969–1981; b) J. Wang, W. Huang, A. Pei, Y. Li, F. Shi, X. Yu, Y. Cui, *Nat. Energy* **2019**, *4*, 664–670.
- [29] L.-P. Hou, X.-Q. Zhang, B.-Q. Li, Q. Zhang, *Angew. Chem. Int. Ed.* **2020**, *59*, 15109–15113.
- [30] B. D. Adams, J. Zheng, X. Ren, W. Xu, J.-G. Zhang, *Adv. Energy Mater.* **2018**, *8*, 1702097.
- [31] M. T. Ribeiro, S. Singh, C. Guestrin, in *Proceedings of the 22nd ACM SIGKDD International Conference on Knowledge Discovery and Data Mining*, Association for Computing Machinery, San Francisco, California, USA, **2016**, pp. 1135–1144.
- [32] N. Yao, L. Yu, Z.-H. Fu, X. Shen, T.-Z. Hou, X. Liu, Y.-C. Gao, R. Zhang, C.-Z. Zhao, X. Chen, Q. Zhang, *Angew. Chem. Int. Ed.* **2023**, *62*, e202305331.
- [33] N. Yao, X. Chen, X. Shen, R. Zhang, Z.-H. Fu, X.-X. Ma, X.-Q. Zhang, B.-Q. Li, Q. Zhang, *Angew. Chem. Int. Ed.* **2021**, *60*, 21473–21478.
- [34] a) M. J. Frisch, G. W. Trucks, H. B. Schlegel, G. E. Scuseria, M. A. Robb, J. R. Cheeseman, G. Scalmani, V. Barone, G. A. Petersson, H. Nakatsuji, X. Li, M. Caricato, A. V. Marenich, J. Bloino, B. G. Janesko, R. Gomperts, B. Mennucci, H. P. Hratchian, J. V. Ortiz, A. F. Izmaylov, J. L. Sonnenberg, Williams, F. Ding, F. Lipparini, F. Egidi, J. Goings, B. Peng, A. Petrone, T. Henderson, D. Ranasinghe, V. G. Zakrzewski, J. Gao, N. Rega, G. Zheng, W. Liang, M. Hada, M. Ehara, K. Toyota, R. Fukuda, J. Hasegawa, M. Ishida, T. Nakajima, Y. Honda, O. Kitao, H. Nakai, T. Vreven, K. Throssell, J. A. Montgomery Jr., J. E. Peralta, F. Ogliaro, M. J. Bearpark, J. J.

- Heyd, E. N. Brothers, K. N. Kudin, V. N. Staroverov, T. A. Keith, R. Kobayashi, J. Normand, K. Raghavachari, A. P. Rendell, J. C. Burant, S. S. Iyengar, J. Tomasi, M. Cossi, J. M. Millam, M. Klene, C. Adamo, R. Cammi, J. W. Ochterski, R. L. Martin, K. Morokuma, O. Farkas, J. B. Foresman, D. J. Fox Gaussian Inc., Wallingford, CT, **2016**; b) A. D. Becke, *J. Chem. Phys.* **1993**, *98*, 5648–5652.
- [35] a) P. Steve, *J. Comput. Phys.* **1995**, *117*, 1–19; b) W. L. Jorgensen, D. S. Maxwell, J. Tirado-Rives, *J. Am. Chem. Soc.* **1996**, *118*, 11225–11236; c) G. A. Kaminski, R. A. Friesner, *J. Phys. Chem. B* **2001**, *105*, 6474–6487.
- [36] a) L. S. Dodda, I. C. de Vaca, J. Tirado-Rives, W. L. Jorgensen, *Nucleic Acids Res.* **2017**, *45*, W331–W336; b) A. V. Marenich, S. V. Jerome, C. J. Cramer, D. G. Truhlar, *J. Chem. Theory Comput.* **2012**, *8*, 527–541; c) J. Z. Vilseck, J. Tirado-Rives, W. L. Jorgensen, *J. Chem. Theory Comput.* **2014**, *10*, 2802–2812; d) T. Lu, F.-W. Chen, *J. Comput. Chem.* **2012**, *33*, 580–592; e) M. Schauperl, P. S. Nerenberg, H. Jang, L. P. Wang, C. I. Bayly, D. L. Mobley, M. K. Gilson, *Commun. Chem.* **2020**, *3*, 44.
- [37] K. P. Jensen, W. L. Jorgensen, *J. Chem. Theory Comput.* **2006**, *2*, 1499–1509.
- [38] L. Martinez, R. Andrade, E. G. Birgin, J. M. Martinez, *J. Comput. Chem.* **2009**, *30*, 2157–2164.
- [39] a) W. G. Hoover, *Phys. Rev. A* **1985**, *31*, 1695–1697; b) S. Nose, *Mol. Phys.* **1984**, *52*, 255–268.
- [40] M. Parrinello, A. Rahman, *J. Appl. Phys.* **1981**, *52*, 7182–7190.
- [41] J. A. Dean, *Lange's Handbook of Chemistry*, 15th ed., McGraw-Hill, New York, **1999**.
- [42] T. Sander, J. Freyss, M. von Korff, C. Rufener, *J. Chem. Inf. Model.* **2015**, *55*, 460–473.

Manuscript received: May 11, 2024

Accepted manuscript online: June 27, 2024

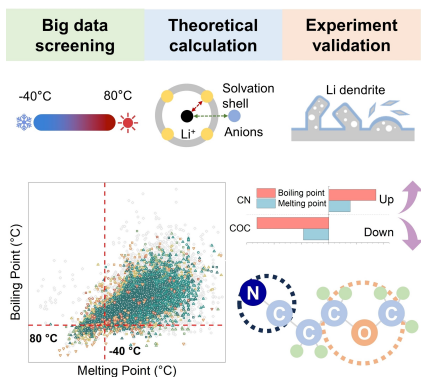
Version of record online: ■■■

Research Article

Molecular Design for Batteries

T. Qin, H. Yang, L. Wang, W. Xue, N. Yao,
Q. Li,* X. Chen,* X. Yang, X. Yu,* Q. Zhang,
H. Li e202408902

Molecule Design for Non-Aqueous Wide-Temperature Electrolytes via the Intelligentized Screening Method



An artificial intelligence (AI)-assisted workflow of wide-temperature electrolyte design is presented. Based on an explainable method, the halogenoid property of the cyanide group is demonstrated similar to fluorine in molecular properties. 3-methoxypropionitrile (MPN) has been determined as a main electrolyte solvent, enabling the LiCoO₂/Li cell operation from -60 to 120 °C.